Predicting Mixture Phase Equilibria and Critical Behavior Using the SAFT-VRX Approach

Lixin Sun,[†] Honggang Zhao,[†] Sergei B. Kiselev,[‡] and Clare McCabe*,[†]

Department of Chemical Engineering, Vanderbilt University, Nashville, Tennessee 37235-1604, and Department of Chemical Engineering, Colorado School of Mines, Golden, Colorado 80401

Received: December 8, 2004; In Final Form: February 24, 2005

The SAFT-VRX equation of state combines the SAFT-VR equation with a crossover function that smoothly transforms the classical equation into a nonanalytical form close to the critical point. By a combininations of the accuracy of the SAFT-VR approach away from the critical region with the asymptotic scaling behavior seen at the critical point of real fluids, the SAFT-VRX equation can accurately describe the global fluid phase diagram. In previous work, we demonstrated that the SAFT-VRX equation very accurately describes the $p\upsilon T$ and phase behavior of both nonassociating and associating pure fluids, with a minimum of fitting to experimental data. Here, we present a generalized SAFT-VRX equation of state for binary mixtures that is found to accurately predict the vapor−liquid equilibrium and $p\upsilon T$ behavior of the systems studied. In particular, we examine binary mixtures of *n*-alkanes and carbon dioxide + *n*-alkanes. The SAFT-VRX equation accurately describes not only the gas−liquid critical locus for these systems but also the vapor−liquid equilibrium phase diagrams and thermal properties in single-phase regions.

1. Introduction

Detailed knowledge of the thermodynamic properties and phase behavior of fluid mixtures is essential for the accurate design and analysis of chemical processes.[1] Although experimental measurements are available for common fluid mixtures, experimental data for many systems of industrial interest tend to be restricted to low molecular weight molecules and over limited regions of the phase diagram. The development of predictive thermodynamic models therefore remains an active research area. A particular challenge in this endeavor is achieving the combination of accuracy both near to and far from the critical point. In the current drive to replace volatile organic solvents in industrial chemical processes with environmentally benign ones, accurate predictions of the thermodynamics and phase behavior of supercritical fluids, such as water, carbon dioxide, and their mixtures, is key to the development of alternative supercritical technologies. Toward the goal of an accurate equation of state for the global fluid phase diagram, in previous work we developed the SAFT-VRX equation of state. SAFT-VRX combines the classical SAFT-VR equation with a crossover function that smoothly transforms the classical equation of state into the correct nonanalytical form close to the critical point.[2,3] We demonstrated the accuracy of the SAFT-VRX approach in describing the fluid phase behavior of associating and nonassociating pure fluids, both far from and in the critical region through application to carbon dioxide, water, and *n*-alkanes, where we developed simple relations to determine the SAFT-VRX parameters for hydrocarbons without fitting to experimental data.[2,3] Here, we extend the SAFT-VRX equation to mixtures.

When theoretical models to predict the thermodynamic properties of mixtures are established, consideration should be given to the shape and size differences between the pure components. While simple cubic equations of state (EOS), such as those proposed by Redlich and Kwong,[4] Soave,[5] Peng and Robinson,[6] and other empirical modifications,[7] represent the thermodynamic properties of pure fluids and fluid mixtures more accurately than the classical, two-parameter van der Waals EOS, these equations do not consider the real size and shape of molecules and are not thermodynamically self-consistent, therefore limiting their predictive capabilities. The SAFT[8,9] equation, based on Weitherm's first-order perturbation theory for association,[10−15] has proven to be a very versatile theoretical model. The SAFT equation has been successfully applied to describe the phase equilibrium of a wide range of industrially important fluids and fluid mixtures (for an overview see the excellent review by Muller and Gubbins[16]). In this work, we focus on the SAFT-VR equation of state, which is a modification of the original SAFT expressions to treat potentials of variable range.[17,18] The SAFT-VR equation has been successfully applied to study several fluids of industrial interest, such as *n*-alkanes and their mixtures,[19−25] polymers,[26,27] perfluoroalkanes,[28−31] carbon dioxide,[32,33] replacement refrigerants,[34] and electrolytes.[35,36] Of particular interest to the current work and in the first application of SAFT-VR to mixtures of real fluids, McCabe et al.[20,21] successfully predicted the phase behavior of binary *n*-alkane mixtures using the SAFT-VR approach with parameters obtained from fitting only to pure component experimental phase equilibrium data. The phase behavior of *n*-alkanes and their mixtures has long been the preferred testing ground for a new equation of state, since abundant and reliable experimental data over wide temperature and pressure ranges is available in the literature. Furthermore, studying *n*-alkanes allows the ability of the equation of state to accurately describe chain molecules to be directly tested before studying more complex systems. In the classification scheme of Scott and van Konynenburg,[37,38] binary mixtures of light alkanes exhibit type I phase behavior (type I phase behavior refers to the phenomena that a continuous

* Author to whom correspondence should be addressed. Phone: (615) 322-6853. Fax: (615) 343-7951. Email: c.mccabe@vanderbilt.edu.
[†] Vanderbilt University.
[‡] Colorado School of Mines.

10.1021/jp044413o CCC: $30.25
Published on Web 04/09/2005

gas−liquid critical locus exists between the critical points of two pure components and no liquid−liquid immiscibility is present). However, a type I system is only observed for binary mixtures in which the ratio of the critical points of the pure components is less than a certain value. For example, binary mixtures of methane + *n*-alkanes first show partial liquid−liquid immiscibility and type V phase behavior with *n*-hexane.[39] With the SAFT-VR approach, McCabe and co-workers[21] were able to accurately predict the transition from type I to type V phase behavior exhibited by the methane + *n*-hexane binary mixture, without fitting any parameters to experimental mixture data. More recently, Galindo and Blas[32,33] have systematically studied the continuous transition of phase behavior from type I to types II, III, and IV for carbon dioxide + *n*-alkane binary mixtures with SAFT-VR. Binary mixtures of CO_2 + *n*-alkanes shorter than *n*-hexane also exhibit type I phase behavior, with partial immiscibility observed for longer *n*-alkane chains. In both of these previous studies, the pure component SAFT-VR parameters were optimized by fitting to experimental vapor pressure and saturated liquid density data and then rescaled to the experimental pure fluid critical points.[39−41] The rescaled parameters allow the high-pressure critical lines to be studied, since the optimized parameters significantly overestimate the gas−liquid critical point. This is because asymptotically close to the critical point the SAFT-VR equation, being analytical in the free energy, cannot reproduce the nonanalytical scaling behavior associated with long-range fluctuations in density seen at the critical point of real fluids and their mixtures.[42] However, while good agreement is obtained for the critical temperatures and pressures with rescaled parameters, agreement with experimental data is lost away from the critical region and also in the prediction of the single-phase and saturated liquid densities. The need to use two sets of parameters to accurately describe the whole phase diagram motivated the development of the SAFT-VRX equation of state.

Nonanalytic scaling equations[42] can correctly describe the thermodynamic properties of pure fluids in the critical region. However, they fail to reproduce the ideal gas limit and are not truly global equations.[43,44] Over the last two decades, a number of approaches to develop global equations of state for fluids have been proposed. These incorporate into the classical equation of state a *crossover function* to satisfy the scaling laws in the critical region. The earliest so-called crossover equation of state was introduced by Chapela and Rowlinson[45] who introduced a switch function to suppress the analytic function in the critical region and the scaling function far away from the critical region. However, like other early approaches, such a combination of the scaling and analytic functions encountered discontinuities in the crossover region.[46] A more rigorous method based on the fundamental results of renormalization group theory was developed by Sengers and co-workers[47−49] and by Kiselev and co-workers.[43,50,51] This approach treats the critical point as the starting point, and upon moving away from the critical point to the low-density regions, the asymptotic quantities from the Ising model are modified to reflect the transition from scaling behavior to classical behavior. Early applications of this approach to cubic equations of state showed that by incorporating the crossover formulation into a classical EOS a good description of the entire phase diagram can be achieved.[43,52] Subsequently, a crossover equation of state for nonassociating[50,53,54] and associating fluids[55] based on the SAFT expressions of Huang and Radosz[56,57] (SAFT-HR) was developed by Kiselev and co-workers. The crossover SAFT-HR equation of state was applied to alkanes,[50] refrigerants,[58] and more recently to eight common supercritical fluids by Hu and co-workers.[59] While the crossover formulation improves the theoretical description in the vicinity of the critical point compared to the classical equation of state alone, deviations from experimental data are in general observed at lower temperatures, which can be attributed to the SAFT-HR equation. The need for an accurate underlying classical EOS, such as the SAFT-VR equation, was clearly demonstrated by McCabe and Kiselev with the development of the SAFT-VRX equation.[60] In a series of papers, the SAFT-VRX approach was shown to provide an excellent description of the $p\nu T$ and phase behavior for both low and high molecular weight alkanes, carbon dioxide, and water.[60,61] Alternative crossover approaches, such as the theoretically founded hierarchical reference theory by Parola and co-workers [62−66] and the globalized renormalization group theory by White and others,[67−71] have also been incorporated into classical equations of state. In particular, the "globalized" renormalization group procedure proposed by White and co-workers[67−71] has been used by Jiang and Prausnitz in a crossover version of their molecular-based equation of state for non-associating chain fluids (EOSCF)[72−75] and by Llovell and co-workers in a crossover version of the soft-SAFT equation of state.[76] However, while these approaches require fewer microscopic intermolecular interaction parameters as input, the resulting equation of state is not formulated in a closed mathematical form and so can only be solved numerically, requiring additional spline functions for the practical representation of the thermodynamic surface of real fluids.

Similar to pure fluids, crossover models that incorporate scaling laws in the critical region and transform into analytic equations away from the critical point are needed to describe the global fluid phase diagram of mixtures. Several different theoretical scaling-law mixture models have been developed for this purpose.[77−88] For example, the Leung−Griffths model suggested that the thermodynamic potential of a near-critical mixture is a smooth function of thermodynamic fields and possesses a singularity that is a universal function of the field variables. This approach has been successfully applied to describe the phase equilibrium surfaces of a number of binary mixtures close to the critical point[80] and was later combined by Belyakov and co-workers with a new parametric crossover model for the transition from scaling-law to regular classical behavior.[89] A more extensive parametric crossover model in the form of the Helmholtz free energy was developed by Kiselev and others,[90−95] which is equally applicable to any pure fluid and binary mixture in the critical region. However, since this approach is an asymptotic crossover model developed for describing the critical region, the equation fails to reproduce the ideal gas law at low densities. A more general procedure for incorporating the scaling laws into any classical equation of state for mixtures was later proposed by Kiselev and Friend.[51] This method presents a closed, self-consistent, thermodynamic model in the form of the Helmholtz free energy and for binary mixtures has successfully been combined with the Patel−Teja[54,96] equation of state, where binary mixtures of methane + ethane and carbon dioxide + ethane and *n*-butane were studied, and with the SAFT-HR equation to study refrigerant mixtures.[58]

In this work, we incorporate crossover theory into the SAFT-VR equation for mixtures by following the approach of Kiselev and Friend.[51,60,61] The accuracy of the SAFT-VRX equation is then demonstrated through prediction of the thermodynamic properties of *n*-alkane and carbon dioxide + *n*-alkane binary mixtures. We proceed as follows. In section 2, we outline the

SAFT-VRX equation for mixtures. In section 3, we describe the results for the *n*-alkane and carbon dioxide + *n*-alkane binary mixtures studied, and comparisons are made with the classical SAFT-VR equation and experimental data. Finally, concluding remarks are made in section 4.

2. Molecular Theory and Models

In the SAFT-VRX approach, chain molecules are described by *m* hard-spherical segments of diameter σ tangentially bonded together. In this united atom approach, each segment represents a group of atoms, which retains the main topological attributes of the chain molecule structure, while simplifying the calculations. The attractive interactions between the segments are incorporated via a potential of variable range, such as the square-well potential

$$u_{ij}(r_{ij}) = \begin{cases} 0 & r_{ij} \geq \lambda_{ij}\sigma_{ij} \\ -\varepsilon_{ij} & \sigma_{ij} \leq r_{ij} < \lambda_{ij}\sigma_{ij} \\ +\infty & r_{ij} < \sigma_{ij} \end{cases} \quad (1)$$

where r_{ij} is the distance, σ_{ij} is the hard-sphere diameter, and λ_{ij} and ϵ_{ij} are the range and depth, respectively, of the attractive potential between two monomer segments *i* and *j*. While the square-well potential has been used in this work, one should note that this is a general approach and other potential forms can be used.

2.1. SAFT-VR. The dimensionless Helmoltz free energy for a fluid mixture of associating chain molecules from the SAFT-VR equation is given by

$$a(T, \upsilon, x_i) = \frac{A}{NkT} = a^{\text{ideal}} + a^{\text{mono}} + a^{\text{chain}} + a^{\text{assoc}} = a^{\text{ideal}} + a^{\text{res}} \quad (2)$$

where a^{ideal} is the ideal free energy, a^{mono} is the excess free energy due to the monomer segments, a^{chain} is the contribution from the formation of chains, and a^{assoc} is the contribution due to association, which is not presented in this work since we do not consider mixtures of associating fluids. a^{res} refers to the residual part of Helmholtz free energy and is given by

$$a^{\text{res}} = a^{\text{mono}} + a^{\text{chain}} + a^{\text{assoc}} \quad (3)$$

We note that all quantities in eq 2 are functions of temperature *T*, molar volume υ, and the composition vector $\{x_i\}$. We briefly describe each contribution in turn.

Ideal Contribution. The ideal Helmholtz free energy for a mixture with *n* components is given by[97]

$$a^{\text{ideal}} = \left(\sum_{i=1}^{n} x_i \ln \rho_i \Lambda_i^3\right) - 1 \quad (4)$$

where *n* is the number of species, $\rho_i = N_i/V$ is the molecular number density, x_i is the mole fraction, and Λ_i is the thermal de Broglie wavelength of component *i*.

Monomer Contribution. The free energy of a mixture of monomers is written as

$$a^{\text{mono}} = \left(\sum_{i=1}^{n} x_i m_i\right)\frac{A^{\text{M}}}{N_s kT} = \left(\sum_{i=1}^{n} x_i m_i\right) a^{\text{M}} \quad (5)$$

where m_i is the number of monomer segments of component *i* and N_s is total number of segments. The monomer energy per segment of the mixture, a^{M}, is obtained from the Barker and Henderson high-temperature perturbation theory through expansion about the hard-sphere (HS) reference system[98−100]

$$a^{\text{M}} = a^{\text{HS}} + \beta a_1 + \beta^2 a_2 + \ldots \quad (6)$$

where $\beta = 1/kT$ and a_1 and a_2 are the first and second perturbation terms associated with the attractive energy $-\epsilon_{ij}$. The Helmholtz free energy of the HS reference mixture, a^{HS}, is obtained from the expression of Boublik[101] and Mansoori et al.[102] as

$$a^{\text{HS}} = \frac{6}{\pi\rho_s}\left[\left(\frac{\xi_2^3}{\xi_3^2} - \xi_0\right)\ln(1-\xi_3) + \frac{3\xi_1\xi_2}{1-\xi_3} + \frac{{\xi_2}^3}{\xi_3(1-\xi_3)^2}\right] \quad (7)$$

where $\rho_s = N_s/V = \rho(\sum_{i=1}^{n} x_i m_i)$ is the total number density of spherical segments and the reduced densities ξ_l are defined by

$$\xi_l = \frac{\pi}{6}\rho_s\left[\sum_{i=1}^{n} x_{s,i}(\sigma_i)^l\right] \qquad l = 1, 2, 3 \quad (8)$$

where ξ_3 is the overall packing fraction of the mixture. In eq 8, σ_i is the hard-core diameter of a spherical segment in chain *i* and $x_{s,i}$ is the mole fraction of spheres of component in the mixture, given by

$$x_{s,i} = \frac{m_i x_i}{\sum_{k=1}^{n} m_k x_k} \quad (9)$$

When dealing with mixtures based on equations for pure fluids, appropriate mixing rules are necessary to specify the composition dependence. In this work we adopted the van der Waals one-fluid mixing rule,[103,104] which assumes simple relationships between the pair correlation functions for mixtures and those of the pure components. The following definitions for the size, energy, and potential range parameters σ_x, ϵ_x, and λ_x are therefore used

$$\sigma_x^3 = \sum_{i=1}^{n}\sum_{j=1}^{n} x_{s,i}x_{s,j}\sigma_{ij}^3 \quad (10)$$

$$\epsilon_x = \frac{\sum_{i=1}^{n}\sum_{j=1}^{n} x_{s,i}x_{s,j}\epsilon_{ij}\lambda_{ij}^3\sigma_{ij}^3}{\sum_{i=1}^{n}\sum_{j=1}^{n} x_{s,i}x_{s,j}\lambda_{ij}^3\sigma_{ij}^3} \quad (11)$$

$$\lambda_x^3 = \frac{\sum_{i=1}^{n}\sum_{j=1}^{n} x_{s,i}x_{s,j}\epsilon_{ij}\lambda_{ij}^3\sigma_{ij}^3}{\sum_{i=1}^{n}\sum_{j=1}^{n} x_{s,i}x_{s,j}\epsilon_{ij}\sigma_{ij}^3} \quad (12)$$

where variables with subscript *ij* refer to the pair interaction between components *i* and *j*. Here, we choose to implement the mixing rule only in the perturbation terms for the monomer interactions, which corresponds to the MX1b mixing rule of

Galindo et al.[18] Hence, the mean-attractive energy a_1 for square-well molecules, with g_{ij}^{HS} approximated by the radial distribution function for a pure fluid, is given as

$$a_1 = -\frac{2}{3}\rho_s \pi \sum_{i=1}^{n}\sum_{j=1}^{n} x_{s,i}x_{s,j}\epsilon_{ij}\sigma_{ij}^3(\lambda_{ij}^3 - 1)g_0^{HS}[\sigma_x; \xi_x^{eff}(\lambda_{ij})] \quad (13)$$

and the first fluctuation term in the free energy is given by

$$a_2 = -\frac{2}{3}\rho_s K^{HS}\sum_{i=1}^{n}\sum_{j=1}^{n} x_{s,i}x_{s,j}\epsilon_{ij}\alpha_{ij}^{VDW}\left\{g_0^{HS}[\sigma_x; \xi_x^{eff}(\lambda_{ij})] + \rho_s\frac{\partial g_0^{HS}[\sigma_x; \xi_x^{eff}(\lambda_{ij})]}{\partial \rho_s}\right\} \quad (14)$$

where K^{HS} is the isothermal compressibility for a mixture of hard spheres obtained from the Percus−Yevick expression[105]

$$K^{HS} = \frac{\xi_0(1-\xi_3)^4}{\xi_0(1-\xi_3)^2 + 6\xi_1\xi_2(1-\xi_3) + 9\xi_2^3} \quad (15)$$

As in the SAFT-VRX approach for pure fluids,[60] the effective packing fraction ξ_x^{eff} is given by the Pade expression proposed by Patel et al.[106]

$$\xi_x^{eff}(\xi_x, \lambda_{ij}) = \frac{c_1(\lambda_{ij})\xi_x + c_2(\lambda_{ij})\xi_x^2}{[1 + c_3(\lambda_{ij})\xi_x^3]^3} \quad (16)$$

with coefficients given by

$$\begin{pmatrix} c_1(\lambda_{ij}) \\ c_2(\lambda_{ij}) \\ c_3(\lambda_{ij}) \end{pmatrix} = \begin{pmatrix} -3.16492 & 13.35007 & -14.80567 & 5.07286 \\ 43.00422 & -191.66232 & 273.89683 & -128.93337 \\ 65.04194 & -266.46273 & 361.04309 & -162.69963 \end{pmatrix} \begin{pmatrix} 1/\lambda_{ij} \\ 1/\lambda_{ij}^2 \\ 1/\lambda_{ij}^3 \\ 1/\lambda_{ij}^4 \end{pmatrix} \quad (17)$$

and the reduced density defined as

$$\xi_x = \frac{\pi}{6}\rho_s \sum_{i=1}^{n}\sum_{j=1}^{n} x_{s,i}x_{s,j}\sigma_{ij}^3 \quad (18)$$

Chain Contribution. The contribution to the free energy due to the formation of chain molecules from square-well segments is given in terms of the contact value of the background correlation function[17,18]

$$y_{ij}^{mono}(\sigma_{ij}) = g_{ij}^{mono}(\sigma_{ij})\, e^{\beta u_{ij}(\sigma_{ij})} \quad (19)$$

which is approximated by

$$a^{chain} = -\sum_{i=1}^{n} x_i(m_i - 1)\ln[g_0^{HS}[\sigma_{ii}; \xi_{ii}^{eff}(\lambda_{ii})] + \beta\epsilon_{ii}g_1^{ii}(\sigma_{ii})] \quad (20)$$

where the term $g_1^{ii}(\sigma_{ii})$ is obtained from a self-consistent calculation of pressure using the Clausius virial theorem and the first derivative of the free energy with respect to the density.[17] For a mixture of square-well molecules, $g_1^{ij}(\sigma_{ij})$ is given by

$$g_1^{ij}(\sigma_{ij}) = \frac{1}{2\pi\epsilon_{ij}\sigma_{ij}^3}\left[3\left(\frac{\partial a_1^{ij}}{\partial \rho_s}\right) - \frac{\lambda_{ij}}{\rho_s}\frac{\partial a_1^{ij}}{\partial \lambda_{ij}}\right] = \beta\epsilon_{ij}\left\{g_0^{HS}[\sigma_x; \xi_x^{eff}(\lambda_{ij})] + (\lambda_{ij}^3 - 1)\frac{\partial g_0^{HS}[\sigma_x; \xi_x^{eff}(\lambda_{ij})]}{\partial \xi_x^{eff}}\left(\frac{\lambda ij}{3}\frac{\partial \xi_x^{eff}}{\partial \lambda_{ij}} - \xi_x^{eff}\frac{\partial \xi_x^{eff}}{\partial \xi_3}\right)\right\} \quad (21)$$

where the contact value of the radial distribution function g_0^{HS} for a reference mixture of hard spheres at an effective packing fraction is defined as

$$g_0^{HS}[\sigma_x; \xi_x^{eff}] = \frac{1 - \xi_x^{eff}/2}{(1 - \xi_x^{eff})^3} \quad (22)$$

Finally, we determine the cross or unlike parameters in eqs 10−18 from the general Lorentz−Berthelot combining rules[104]

$$\sigma_{ij} = \frac{\sigma_{ii} + \sigma_{jj}}{2} \quad (23)$$

$$\epsilon_{ij} = (1 - k_{ij})(\epsilon_{ii}\epsilon_{jj})^{1/2} \quad (24)$$

$$\lambda_{ij} = \zeta_{ij}\frac{\lambda_{ii}\sigma_{ii} + \lambda_{jj}\sigma_{jj}}{\sigma_{ii} + \sigma_{jj}} \quad (25)$$

where the parameters k_{ij} and ξ_{ij} in eqs 24 and 25 are used to adjust the strength and range of the cross interactions, respectively.

2.2. Crossover Function. In developing the crossover SAFT-VR equation of state for mixtures (SAFT-VRX), we follow the procedures proposed by Kiselev.[43,51] Following this approach, one needs to first rewrite the classical expression for the dimensionless Helmholtz free energy in the form

$$a(T, v) = \Delta a(\Delta T, \Delta v) + a_{bg}(T, v) \quad (26)$$

where the background contribution a_{bg} is given as

$$a_{bg}(T, v) = -\Delta v p_0(T) + a_0^{res}(T) + a_0(T) \quad (27)$$

In eqs 26 and 27, the critical or singular part of the Helmholtz free energy, $\Delta a(\Delta T, \Delta v)$, is a function of the dimensionless distance of the temperature from the classical critical temperature T_{0c} ($\Delta T = T/T_{0c} - 1$) and the molar volume from the classical critical molar volume v_{0c} ($\Delta v = v/v_{0c} - 1$), $p_0(T) = p(T, v_{0c})v_{0c}/RT$ the dimensionless pressure, $a_0^{res}(T) = a^{res}(v_{0c}, T)$ the dimensionless residual Helmholtz free energy, and $a_0(T)$ the dimensionless temperature-dependent ideal gas term along the critical isochore, $v = v_{0c}$.

The critical part of the dimensionless Helmholtz free energy, $\Delta a(\Delta T, \Delta v)$, is subject to three critical point conditions

$$\Delta a(\Delta T = 0, \Delta v = 0) = 0 \qquad \left(\frac{\partial \Delta a}{\partial \Delta v}\right)_{\Delta T=0,\Delta v=0} = 0 \qquad \left(\frac{\partial^2 \Delta a}{\partial \Delta v^2}\right)_{\Delta T=0,\Delta v=0} = 0 \quad (28)$$

By solving eqs 2, 26, and 28 simultaneously, we derive

the critical term as

$$\Delta a(\Delta T, \Delta v) = a^{res}(\Delta T, \Delta v) - a_0^{res}(\Delta T) - \ln(\Delta v + 1) + \Delta v p_0(\Delta T) \quad (29)$$

ΔT and Δv in the critical term are then replaced by the renormalized values

$$\bar{\tau} = \tau Y^{-\alpha/2\Delta_1} + (1+\tau)\Delta\tau_c Y^{2(2-\alpha)/3\Delta_1}$$

$$\bar{\varphi} = \varphi Y^{(\gamma-2\beta)/4\Delta_1} + (1+\varphi)\Delta v_c Y^{(2-\alpha)/2\Delta_1} \quad (30)$$

where the universal critical exponents are

$$\alpha = 0.110 \quad \beta = 0.325 \quad \gamma = 2 - \alpha - 2\beta = 1.24 \quad \Delta_1 = 0.51 \quad (31)$$

In eq 30, $\tau = T/T_c - 1$ is the dimensionless deviation of the temperature from the real critical temperature, T_c, $\varphi = v/v_c - 1$ is the dimensionless deviation of the molar volume from the real critical molar volume v_c, and $\Delta\tau_c = \Delta T_c/T_{0c} = (T_c - T_{0c})/T_{0c}$ and $\Delta v_c = \Delta v_c/v_{0c} = (v_c - v_{0c})/v_{0c}$ are the dimensionless shifts between the classical critical temperature T_{0c} and critical volume v_{0c} and the real critical temperature T_c and critical volume v_c. The crossover function Y in eq 30 can be written in parametric form[50,54]

$$Y(q) = \left[\frac{q}{1+q}\right]^{2\Delta_1} \quad (32)$$

where $q = (r/Gi)^{1/2}$ is the renormalized distance from the critical point and $r(\tau, \varphi)$ is a parametric variable. The variable q is related to the order parameter φ and dimensionless temperature τ through the crossover SINE model[50,54]

$$\left(q^2 - \frac{\tau}{Gi}\right)\left[1 - \frac{1}{4}\left(1 - \frac{\tau}{q^2 Gi}\right)\right] = b^2\left(\frac{\varphi}{Gi^\beta}[1 + v_1\varphi^2 \exp(-10\varphi) + d_1\tau]\right)^2 Y^{(1-2\beta)/\Delta_1} \quad (33)$$

In eq 33, Gi is the Ginzburg number for the fluid of interest, $b^2 = 1.359$ is the universal linear-model parameter, and d_1 and v_1 are system-dependent parameters related to the rectilinear diameter and asymmetry of the vapor−liquid envelope.

The final form of the crossover expression for the Helmholtz free energy can be rewritten as

$$a(T, v, x_i) = \Delta a(\bar{\tau}, \bar{\varphi}) - \Delta v p_0(T) + a_0^{res}(T) + a_0(T) \quad (34)$$

where the renormalized critical term is given by

$$\Delta a(\bar{\tau}, \bar{\varphi}) = a^{res}(\bar{\tau}, \bar{\varphi}) - a_0^{res}(\bar{\tau}) - \ln(\bar{\varphi} + 1) + \bar{\varphi} p_0(\bar{\tau}) \quad (35)$$

Equations 34 and 35 represent the SAFT-VRX equation derived by incorporating the crossover transformations defined by eqs 30−33 into the SAFT-VR equation for mixtures. Asymptotically close to the critical point $q \ll 1$, the crossover function behaves as $Y \approx r^{\Delta_1}$, the renormalized temperature as $\bar{\tau} \cong \tau r^{-\alpha/2}$, and the order parameter as $\bar{\varphi} \cong \varphi r^{(\gamma-2\beta)/4}$. As a result, the renormalized critical term $\Delta a(\bar{\tau}, \bar{\varphi})$ becomes a nonanalytic function of τ and φ, which after differentiation reproduces the correct scaling laws.[107,108] Far away from the critical point $q \gg 1$, the crossover function behaves as $Y(q) \cong 1$, and the renormalized temperature and order parameter tend to their classical values $\bar{\tau} \to \tau$ and $\bar{\varphi} \to \varphi$. As a result, the renormalized residual free energy is transformed into its classical analogue $\Delta a(\bar{\tau}, \bar{\varphi}) \to \Delta a(\Delta T, \Delta v)$, and all thermodynamic properties exhibit analytical−classical behavior as determined by eq 2. As discussed earlier, we note that composition does not explicitly appear in the SAFT-VRX expressions, though the crossover parameters Gi, d_1, and v_1 are implicit functions of x_i based on the van der Waals one-fluid assumption. When the van der Waals one-fluid theory is implemented, the following simple linear mixing rules are used for the crossover parameters

$$Gi^{-1}(x) = \sum_{i=1}^{n} x_i [Gi^{-1}]^{(i)} \quad (36)$$

$$v_1(x) = \sum_{i=1}^{n} x_i v_1^{(i)} \quad (37)$$

$$d_1(x) = \sum_{i=1}^{n} x_i d_1^{(i)} \quad (38)$$

where the superscript i refers to the pure component value for each parameter.

To calculate the mixture critical line, we need to formulate the equations to be solved for the critical locus. In the SAFT-VRX equation for binary mixtures (unlike for pure fluids[60,61]), the renormalization as given by eq 35 (which appears near the real critical point of the fluid) is determined by the following conditions

$$P(T_c, v_c, \mu_c) = P_c \quad \left(\frac{\partial P}{\partial v}\right)_{T_c, v_c, \mu_c} = 0 \quad \left(\frac{\partial^2 P}{\partial v^2}\right)_{T_c, v_c, \mu_c} = 0 \quad (39)$$

where the chemical potential of the mixture $\mu = (\partial A/\partial x)_{T,v}$. From eq 39, the equation of state for a binary mixture near the critical point should be formulated in terms of the chemical potential. However, this implementation would make the crossover calculations for mixtures very complex, and so in eqs 30−35, following Kiselev and Friend,[51] we use the composition variable x

$$P(T_c, v_c, x_c) = P_c \quad \left(\frac{\partial P}{\partial v}\right)_{T_c, v_c, x_c} = 0 \quad \left(\frac{\partial^2 P}{\partial v^2}\right)_{T_c, v_c, x_c} = 0 \quad (40)$$

In the SAFT-VRX approach, the calculation of the critical shifts (i.e., the deviation of the classical critical point from the real critical point) for pure fluids uses experimental values for the real critical point since they are readily available. For mixtures, experimental data for the critical line is usually only available for simple systems, and the use of experimental critical lines would limit the predictive ability of the approach. Therefore, the critical shifts for the mixtures $\Delta\tau_c$ are obtained from the critical shifts of the pure components $\Delta\tau_c^i$

$$\Delta\tau_c(x) = \sum_i \Delta\tau_c^{(i)} x_i \quad (41)$$

$$\Delta v_c(x) = \sum_i \Delta v_c^{(i)} x_i \quad (42)$$

In turn, the real critical point T_c can now be estimated (i.e., $\Delta\tau_c = (T_c - T_{0c})/T_{0c}$) for use in the renormalization given by eq 30.

3. Results

To demonstrate the accuracy of the SAFT-VRX equation of state for the prediction of mixture fluid phase behavior, we present

TABLE 1: SAFT-VRX Parameters for Carbon Dioxide and the *n*-Alkanes Studied in This Work[a]

	m	σ/Å	λ	$(\epsilon/k_B)/K$	Gi^{-1}	d_1	υ_1
ethane	1.996	3.475	1.627	139.202	7.214	0.458	0.00861
propane	2.377	3.649	1.640	153.235	6.923	0.469	0.00666
n-butane	2.740	3.776	1.647	163.707	6.651	0.480	0.00568
n-pentane	3.094	3.875	1.651	171.886	6.394	0.492	0.00509
n-hexane	3.445	3.958	1.652	178.491	6.150	0.503	0.00470
n-heptane	3.793	4.028	1.653	183.951	5.919	0.514	0.00442
n-octane	4.138	4.090	1.653	188.542	5.700	0.526	0.00421
n-decane	4.825	4.198	1.653	195.812	5.293	0.548	0.00392
n-tridecane	5.850	4.330	1.653	203.452	4.754	0.582	0.00365
n-tetradecane	6.190	4.370	1.653	205.379	4.592	0.594	0.00358
carbon dioxide	2.688	2.724	1.625	124.115	6.053	0.824	0.00550

[a] m is the number of spherical segments in the model, σ is the hard-core diameter, ϵ and λ are the depth and range of the square well, respectively, Gi is the Ginzburg number, and d_1 and υ_1 are crossover parameters.

results for *n*-alkane and carbon dioxide + *n*-alkane binary mixtures. In the SAFT-VRX approach, the SAFT (σ, λ, and ϵ) and crossover parameters (Gi, d_1, and υ_1) for each pure component can be determined from a direct fitting to the experimental data. This approach was followed to derive the parameters for carbon dioxide, which are given in Table 1.[109] In previous work on the pure *n*-alkanes, from a simultaneous optimization of the SAFT-VRX equation to the vapor−liquid equilibrium and $p\upsilon T$ data of selected *n*-alkanes in the C_1-C_{40} range, McCabe and Kiselev[60] developed expressions for both the classical and crossover parameters for pure alkanes as a function of carbon number and molecular weight

$$m = 1 + a_{m,1}(C_m - 1)^{0.1} + a_{m,2}(C_m - 1) \tag{43}$$

$$\lambda = a_{\lambda,0} + a_{\lambda,1}(C_m - 1)^{0.25} + a_{\lambda,2}(C_m - 1) \tag{44}$$

$$m\sigma = a_{\sigma,0} + a_{\sigma,1}(mM_w)^{0.5} + a_{\sigma,2}\left(\frac{mM_w}{1 + a_{\sigma,4}C_m}\right) + a_{\sigma,3}\left(\frac{mM_w}{1 + a_{\sigma,4}C_m}\right)^{0.75} \tag{45}$$

$$m\varepsilon = a_{\varepsilon,0} + a_{\varepsilon,1}(mM_w)^{0.5} + a_{\varepsilon,2}(mM_w)^{0.75} + a_{\varepsilon,3}(mM_w) \tag{46}$$

$$Gi^{-1} = a_{g,0} + a_{g,1}(C_m) + a_{g,2}(C_m)^{1.5} \tag{47}$$

$$\upsilon_1 = \frac{a_{\upsilon,0} + a_{\upsilon,1}C_m}{1 + a_{\upsilon,2}C_m} \tag{48}$$

$$d_1 = a_{d,0} + a_{d,1}C_m \tag{49}$$

where C_m is the number of carbon atoms in the *n*-alkane chain, M_w the molecular weight, and $a_{x,i}$ are fitted coefficients where $x = m$, λ, σ, ϵ, g, υ, or d. The critical shifts for the pure components are expressed as functions of the Ginzburg number Gi

$$\Delta\tau_c = -\frac{\delta_\tau Gi}{1 + Gi} \tag{50}$$

$$\Delta\upsilon_c = -\frac{\delta_\eta Gi}{1 + Gi} \tag{51}$$

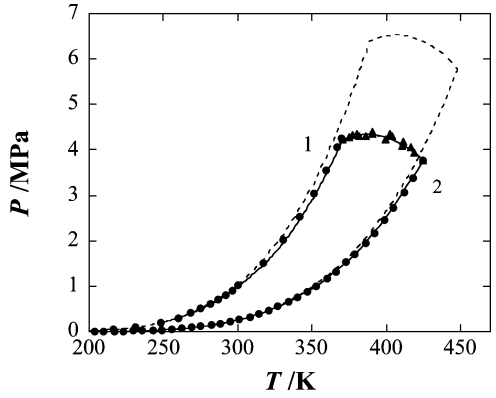

Figure 1. $p-T$ projection of the propane (1) + *n*-butane (2) phase diagram. The solid lines correspond to predictions from the SAFT-VRX equation, and the dashed lines predictions from the SAFT-VR equation with optimized parameters.[19] The solid triangles correspond to experimental gas−liquid critical data,[112] and the solid circles experimental vapor pressures for the pure components.[121]

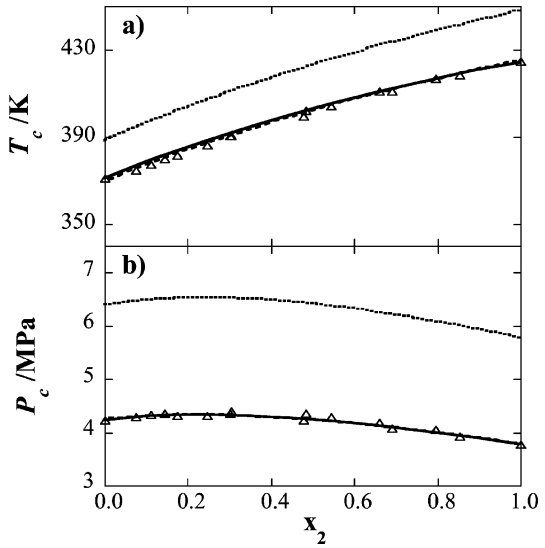

Figure 2. (a) T_c-x_2 and (b) P_c-x_2 projections of the gas−liquid critical line for the propane (1) + *n*-butane (2) phase diagram. The solid line corresponds to the SAFT-VRX prediction, the dashed line the SAFT-VR prediction obtained from rescaled parameters, and the dotted line from the SAFT-VR equation with optimized parameters. The triangles correspond to the experimental data.[122−125]

with coefficients $\delta_\eta = 2.086$ for *n*-alkanes and $\delta_\eta = 1.847$ for carbon dioxide. In both cases, $\delta_\tau = 0$.

We first present results for the binary *n*-alkane systems. In Figure 1, the $p-T$ projection of the propane (1) + *n*-butane (2) binary mixture is presented. For comparison, the predictions for both the pure fluids and the binary mixture from the SAFT-VR equation with parameters optimized to the vapor pressure curves and saturated liquid densities of the pure components are also included (predictions from SAFT-VR with rescaled parameters are not included as they would be indistinguishable from the SAFT-VRX prediction in this representation of the phase diagram). As was seen in preliminary studies of light *n*-alkanes,[110] the SAFT-VRX prediction for the binary fluid phase behavior is in very good agreement with the experimental data. We note that the results presented in this figure represent true predictions, because the Lorentz−Berthelot combining rules are used to determine the cross interactions and no binary experimental data was used to optimize the prediction of the phase diagram from either the SAFT-VRX or SAFT-VR approach. For the same system, in Figure 2 we show the gas−

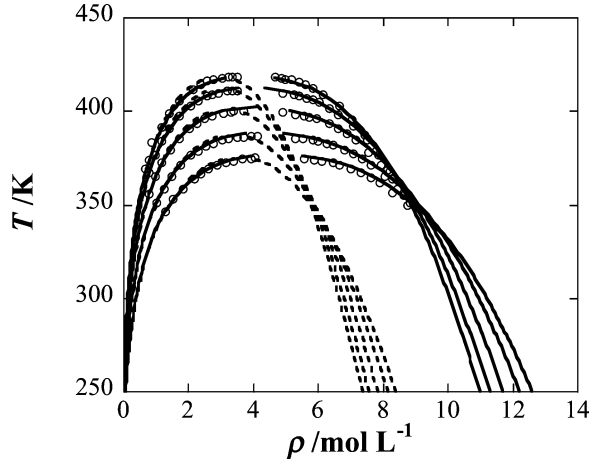

Figure 3. Constant x $T-\rho$ slices of the *n*-propane (1) + *n*-butane (2) phase diagram at $x_2 = 0.8532$, 0.6915, 0.4789, 0.2455, and 0.0742 (from top to bottom). The solid lines correspond to the SAFT-VRX predictions, the dashed lines the SAFT-VR predictions with rescaled parameters,[22] and the symbols experimental data.[124]

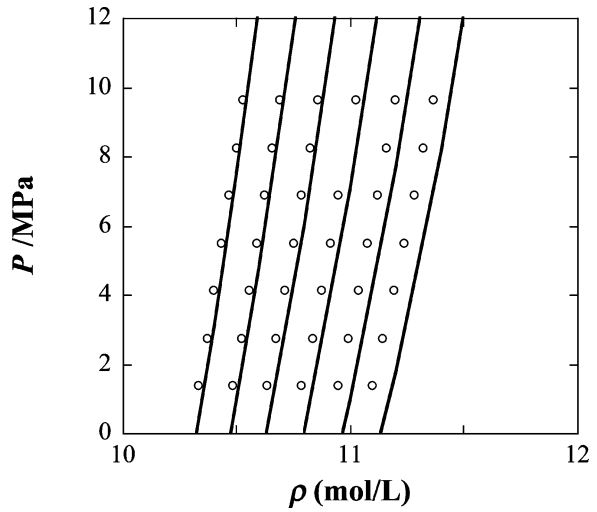

Figure 4. Comparison of predicted $p\rho T$ data for propane (1) + *n*-butane (2) binary mixtures at $T = 283.15$ K and $x_2 = 0.8984$, 0.7999, 0.6999, 0.6004, 0.4988, and 0.3992 (from left to right) with experimental data. The solid lines correspond to the SAFT-VRX predictions, and the symbols the experimental data.[111]

liquid critical lines as a function of composition as predicted from the SAFT-VRX and SAFT-VR equations, with both optimized and rescaled parameters. As expected, both the SAFT-VRX and rescaled SAFT-VR equations give very good descriptions of the critical temperature and critical pressure as a function of composition, while the SAFT-VR prediction using optimized parameters significantly overpredicts the experimental data. To demonstrate the advantage of the SAFT-VRX equation in Figure 3, we present constant composition $T-\rho$ slices of the propane (1) + butane (2) phase diagram. From the figure, we see that the SAFT-VRX equation accurately predicts the experimental phase behavior for each binary mixture studied both far from and in the critical region. The problem with the classical SAFT-VR equation is also clearly illustrated; with the rescaled parameters, the classical equation significantly underpredicts the experimental liquid densities. Therefore, while the rescaled parameters accurately describe the critical line in $p-T$ space, they cannot be used to study the density dependence. If the optimized SAFT-VR parameters were used, then the agreement with the experimental data would be recovered away from the critical region, though the critical point would be over estimated.

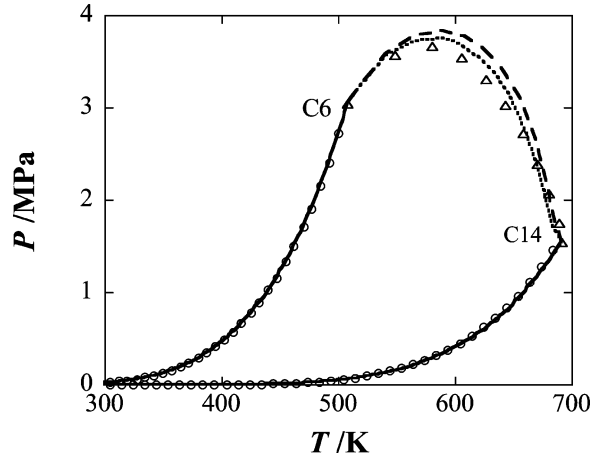

Figure 5. $p-T$ projection for the *n*-hexane (1) + *n*-tetradecane (2) binary mixture from the SAFT-VRX equation of state compared with experimental data. The triangles represent the experimental gas−liquid critical points,[126] and the circles the experimental vapor pressures for the pure components.[121] The solid curves correspond to the SAFT-VRX prediction for the pure component vapor pressures, the dashed line the predicted critical line from the mixture SAFT-VRX approach with $\tau_{ij} = 0$, and the dotted line the predicted mixture SAFT-VRX critical line with $\tau_{ij} = 0.03$.

TABLE 2: Recommended Values for the Parameter τ_{Ij} in Eq 52

mixture	τ_{ij}	mixture	τ_{ij}
$C_2H_6 + n\text{-}C_4H_{10}$	0	$n\text{-}C_6H_{14} + n\text{-}C_7H_{16}$	0
$C_2H_6 + n\text{-}C_6H_{14}$	0.025	$n\text{-}C_6H_{14} + n\text{-}C_8H_{18}$	0.010
$C_3H_8 + n\text{-}C_4H_{10}$	0	$n\text{-}C_6H_{14} + n\text{-}C_{10}H_{22}$	0.025
$C_3H_8 + n\text{-}C_6H_{14}$	0.015	$n\text{-}C_6H_{14} + n\text{-}C_{13}H_{28}$	0.03
$n\text{-}C_4H_{10} + n\text{-}C_5H_{12}$	0	$n\text{-}C_6H_{14} + n\text{-}C_{14}H_{30}$	0.03
$n\text{-}C_4H_{10} + n\text{-}C_6H_{14}$	0.010	$C_2H_6 + CO_2$	0.03
$n\text{-}C_4H_{10} + n\text{-}C_7H_{16}$	0.015	$C_3H_8 + CO_2$	0.04
$n\text{-}C_4H_{10} + n\text{-}C_8H_{18}$	0.025	$n\text{-}C_4H_{10} + CO_2$	0.06
$n\text{-}C_5H_{12} + n\text{-}C_9H_{20}$	0.025	$n\text{-}C_5H_{10} + CO_2$	0.08

The SAFT-VRX equation can also be used to predict single-phase pVT behavior. Comparison of the SAFT-VRX predictions with the experimental data of Parrish[111] for the propane (1) + *n*-butane (2) binary mixture is presented in Figure 4. At various compositions, the SAFT-VRX approach is found to predict the experimental $p\rho T$ data well, while the SAFT-VR predictions with optimized or rescaled parameters show much larger deviations.

The SAFT-VRX approach can also be used to predict the phase behavior of binary mixtures of longer hydrocarbon chains. In Figure 5, we show the $p-T$ projection for the *n*-hexane (1) + *n*-tetradecane (2) binary mixture. From the figure, we note that the SAFT-VRX equation slightly overpredicts the experimental critical locus (dashed line). This is a direct consequence of the simplification made in the SAFT-VRX approach for mixtures to develop a predictive approach that does not require the experimental mixture critical points as input; in eqs 41 and 42, we use the critical shifts for the pure components to estimate the critical shifts for the mixtures rather than the experimental critical line, and as the two pure components become more dissimilar, the simple composition-based combining rules become less accurate. To correct this behavior, we introduce an adjustable parameter, τ_{ij}, into eq 41

$$\Delta\tau_c(x) = \sum_i \Delta\tau_c^{(i)} x_i + \sum_i x_i \sum_j x_j \tau_{ij} \qquad (52)$$

While τ_{ij} can be adjusted to fit experimental data, we have found that it is possible to predetermine the value needed based on

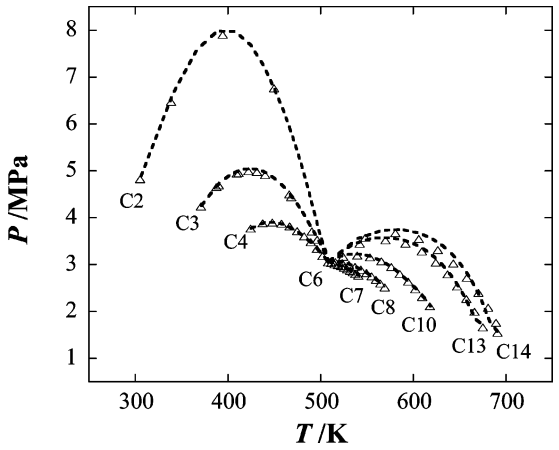

Figure 6. Comparison of the predicted gas−liquid critical lines for binary mixtures of *n*-hexane + *n*-alkanes from the SAFT-VRX approach with experimental data. The triangles represent experimental data,[112] and the dashed lines the theoretical predictions from the SAFT-VRX approach.

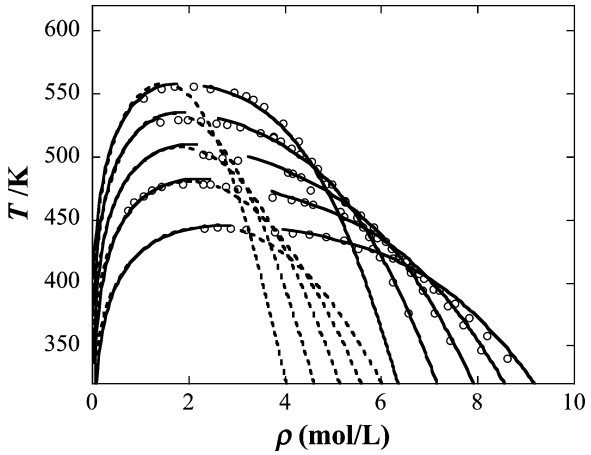

Figure 7. Constant x $T-\rho$ slices of the *n*-butane (1) + *n*-octane (2) phase diagram at $x_2 = 0.8177$, 0.5369, 0.3291, 0.1817, and 0.0539 (from top to bottom). The solid lines correspond to the SAFT-VRX predictions, and the symbols experimental data.[127]

the difference in carbon number between the two pure components (Table 2). For binary mixtures of low molecular weight alkanes (methane to propane), and when the difference in carbon number between the two components is 1, a τ_{ij} is not needed. For binary mixtures of longer *n*-alkane chains, the following values are recommended: for carbon number differences of 2, $\tau_{ij} = 0.01$; for a difference in carbon number of 3, $\tau_{ij} = 0.015$; for differences of 4 and 5, $\tau_{ij} = 0.025$; and for differences of 6−8, τ_{ij} 0.03. For higher chain length differences, we anticipate similar guidelines will hold, though the maximum difference in carbon number studied in this work was 8. Therefore, for the *n*-hexane (1) + *n*-tetradecane (2) binary mixture where the difference in carbon number between the two pure components is 8, we see that the SAFT-VRX prediction using a τ_{ij} of 0.03 significantly improves the prediction of the gas−liquid critical locus. To demonstrate the accuracy of the SAFT-VRX approach for long-chain *n*-alkane mixtures, with the τ_{ij} parameter determined using the prescriptions above, the $p-T$ projection for nine *n*-hexane + *n*-alkane binary mixtures is presented in Figure 6. As can be seen from the figure, the continuous gas−liquid critical lines predicted from the SAFT-VRX approach are in excellent agreement with experimental data. We remind the reader that the Lorentz−Berthelot combining rules have been used to determine the unlike energy and size interactions, and

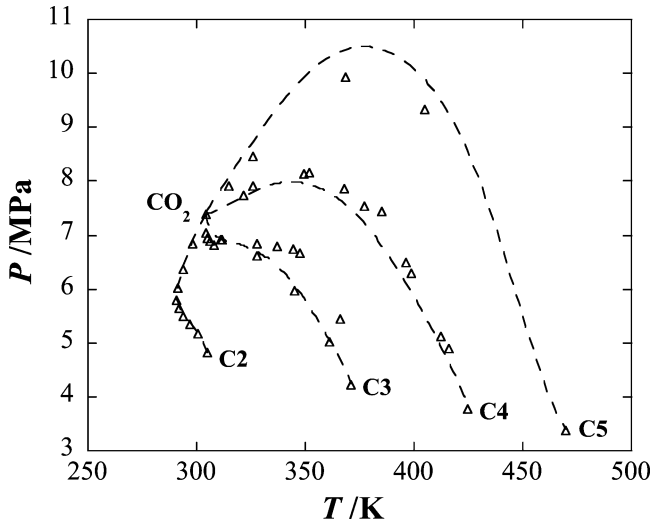

Figure 8. Predicted gas−liquid critical lines for the binary mixtures of carbon dioxide + ethane, propane, *n*-butane, and *n*-pentane compared to experimental data. The symbols represent the experimental data,[112] and the lines the predictions from the SAFT-VRX approach.

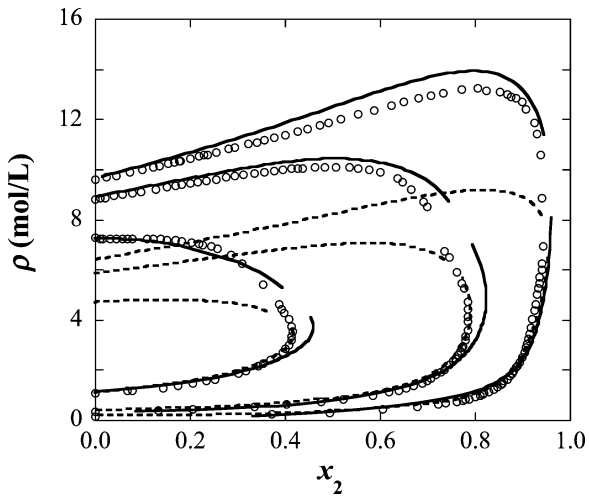

Figure 9. Constant T $\rho-x$ slices of the carbon dioxide (1) + *n*-butane (2) phase diagram at $T = 311.09$, 344.43, and 394.6 K (from right to left). The solid lines correspond to the SAFT-VRX predictions, the dashed lines to predictions form the SAFT-VR equation using rescaled parameters,[33] and the symbols the experimental data.[113]

therefore these results represent predictions of the phase diagram. For the longer *n*-alkane binary mixtures, we again see the advantage of the SAFT-VRX approach over the classical SAFT-VR equation of state when we consider density projections of the phase diagram. In Figure 7, constant composition $T-\rho$ slices of the *n*-butane (1) + *n*-octane (2) phase diagram are presented. The SAFT-VRX approach provides accurate predictions of the phase diagram for each composition of the mixture studied.

We now turn to the carbon dioxide + *n*-alkane binary mixtures studied. Due to the unlike nature of the two pure components, departure form the Lorentz−Berthelot combining rules is observed for these systems. As in the work of Galindo and Blas with the SAFT-VR approach, two unlike parameters k_{ij} and ζ_{ij} are introduced into eqs 24 and 25, respectively, to adjust the cross interactions. In this work, optimized values of $k_{ij} = 0.03$ and $\zeta_{ij} = 0.98$ have been determined for these parameters by fitting to the critical line of the carbon dioxide + ethane binary mixture. These parameters are then used transferably to predict the gas−liquid critical lines for other

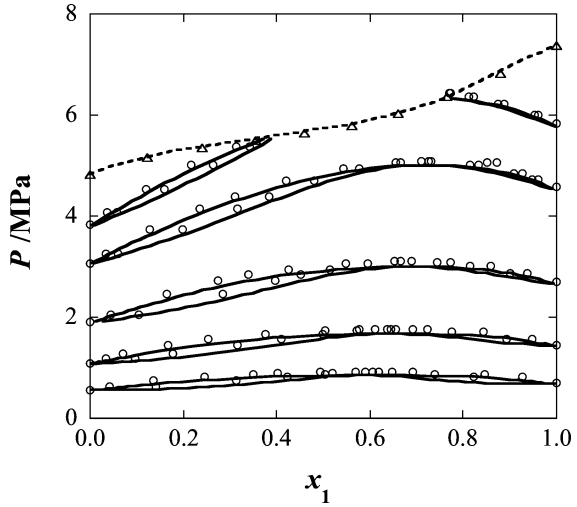

Figure 10. Constant temperature $P-x$ slices for the carbon dioxide (1) + ethane (2) binary mixtures at 293.15, 283.15, 263.15, 243.15, and 223.15 K (from top to bottom). The triangles correspond to the experimental gas−liquid critical point data,[115] and the circles the coexistence curves.[114]

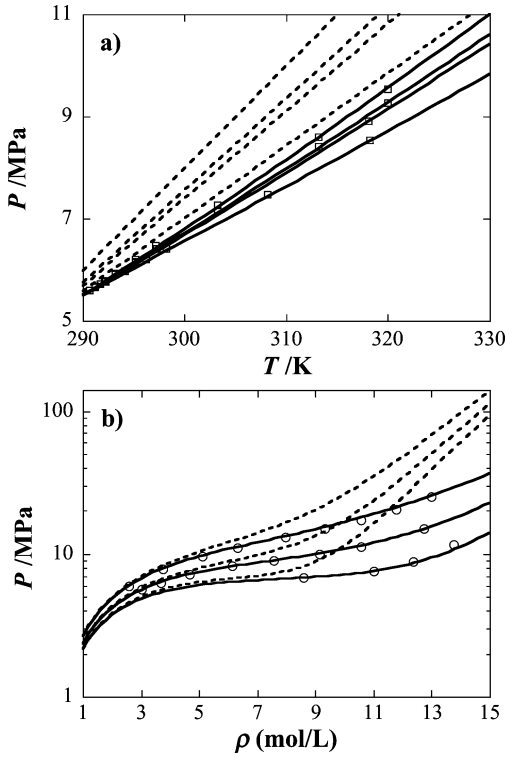

Figure 11. (a). $p-T$ isochors at $\rho = 8.44$, 8.00, 7.79, and 7.05 mol L^{-1} (from top to bottom) and (b) $p-\rho$ isotherms at $T = 350$, 320, and 300 K (from top to bottom) for the carbon dioxide (1) + ethane (2) binary mixtures at $x_1 = 0.508$. The solid lines correspond to the SAFT-VRX predictions, the dashed lines predictions from the SAFT-VR equation using rescaled parameters,[33] the squares experimental data by Weber,[116] and circles experimental data by Lau.[117]

carbon dioxide + *n*-alkane binary mixtures without additional fitting to the experimental data. As for the binary *n*-alkane mixtures, we introduce τ_{ij} into eq 41, which is again found to follow a simple trend with carbon number (Table 2). The predicted SAFT-VRX critical lines for the carbon dioxide + ethane, propane, *n*-butane, and *n*-pentane binary mixtures are presented in Figure 8. As can be seen from the figure, type I phase behavior is observed for the four binary mixtures studied, and the predictions are in good agreement with the experimental

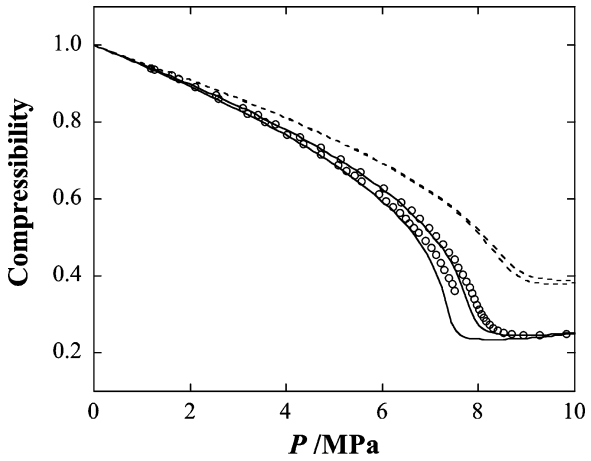

Figure 12. Compressibility data for carbon dioxide (1) + *n*-butane (2) binary mixtures at $T = 310.93$ and 304.65 K (from top to bottom). The solid lines correspond to the SAFT-VRX predictions, the dashed lines to predictions from the SAFT-VR equation with rescaled parameters,[33] and the symbols experimental data by Tsuji et al.[118]

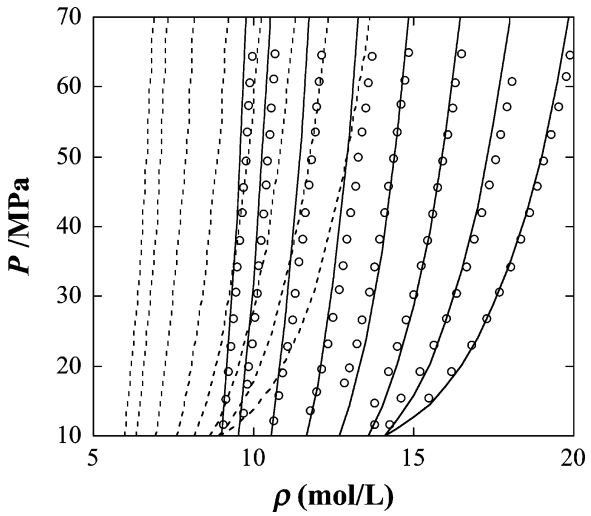

Figure 13. Representation of $p\rho T$ data for the carbon dioxide (1) + *n*-pentane (2) binary mixture at $T = 323$ K and $x_2 = 0.90$, 0.80, 0.65, 0.50, 0.38, 0.28, 0.20, and 0.12 (from left to right). The solid lines correspond to the SAFT-VRX predictions, the dashed lines to predictions from the SAFT-VR equation with rescaled parameters,[33] and the symbols experimental data by Kiran.[119]

data.[112] It is interesting to note that the change in curvature of the gas−liquid critical line from the carbon dioxide + ethane to the carbon dioxide + propane binary mixture, which is related to the minimum azeotropic behavior of the mixture, is predicted precisely by the SAFT-VRX approach. The advantage of the SAFT-VRX approach over the classical equation of state is again illustrated when we focus on the prediction of the whole phase diagram. In Figure 9, we present constant temperature $\rho-x$ slices for the carbon dioxide (1) + *n*-butane (2) binary mixture using the transferable parameters. The SAFT-VRX approach accurately describes the $\rho-x$ coexistence data[113] compared to the SAFT-VR equation. Coexistence curves predicted from the SAFT-VRX equation for the carbon dioxide (1) + ethane (2) binary mixture at several temperatures are compared with experimental data in Figure 10. From the figure, we see that the SAFT-VRX predictions are in good agreement with the experimental data.[114,115] We have also studied the thermal properties in one-phase regions, for the carbon dioxide + ethane, *n*-butane, and *n*-pentane binary mixtures, as examples to demonstrate the strength of the SAFT-VRX equation. Again,

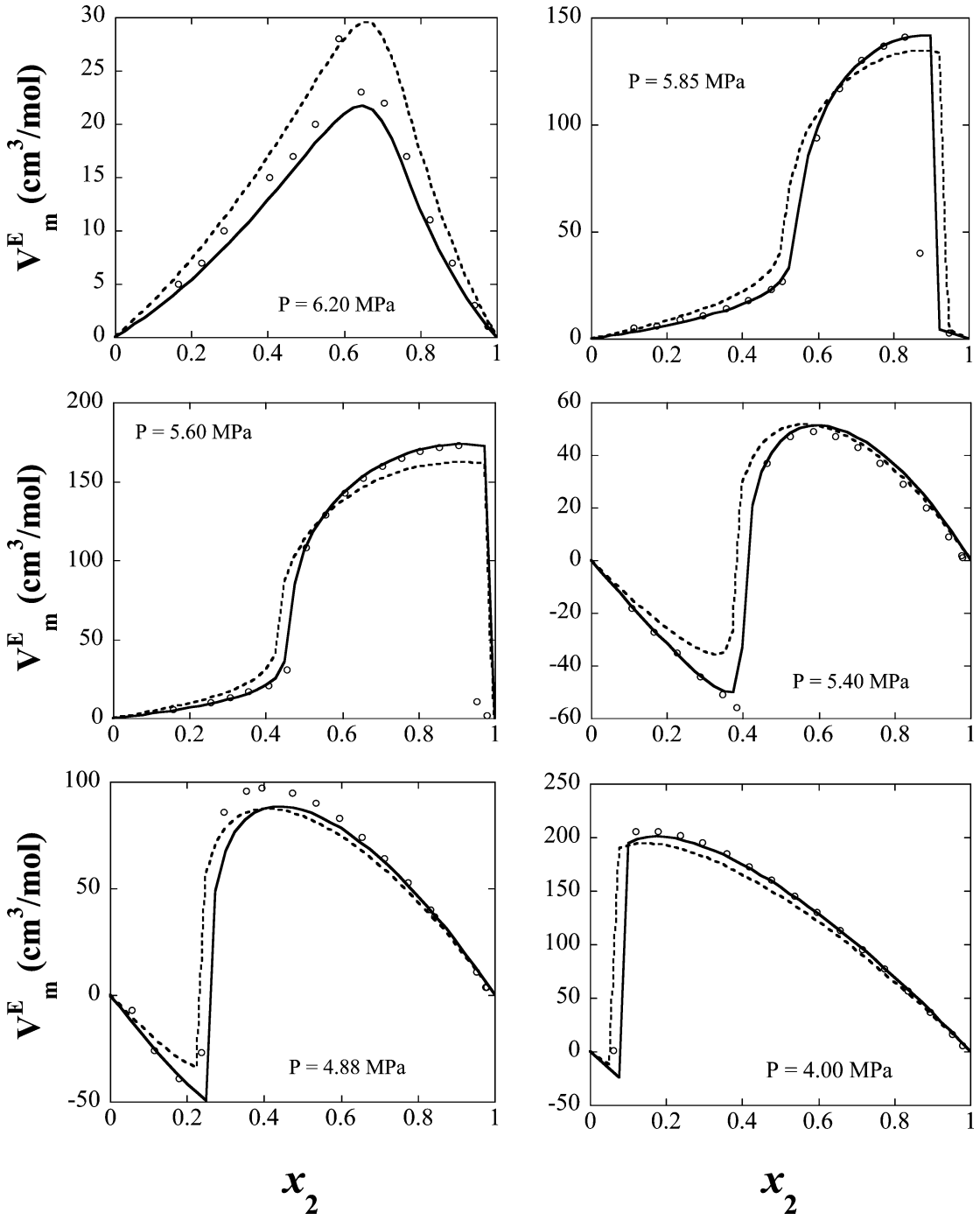

Figure 14. Representation of excess volumes V_m^E for the carbon dioxide (1) + ethane (2) binary mixture at $T = 291.6$ K at $P = 6.20$, 5.85, 5.60, 5.40, 4.88, and 4.00 MPa as a function of composition. The symbols correspond to experimental data,[120] the solid curves predictions from the SAFT-VRX equation, and the dashed curves predictions from SAFT-VR.[33]

for each system we use the cross interaction parameters determined from a fit to the critical line of the carbon dioxide + ethane binary mixture, and therefore the results represent predictions of the phase behavior. A comparison of the predictions from the SAFT-VRX equation and experimental $p\rho T$ data[116,117] for a 49.2% carbon dioxide (1) + ethane (2) binary mixture is presented in Figure 11. In both cases, the SAFT-VRX equation is in much better agreement with the experimental data than the SAFT-VR equation using rescaled parameters. Comparisons are also made between theoretical predictions and experimental compressibility data[118] close to the critical region for the carbon dioxide + *n*-butane binary mixture in Figure 12 and experimental $p\rho T$ data[119] for the carbon dioxide (1) + *n*-pentane (2) mixture in Figure 13. In both cases, the SAFT-VRX approach represents the experimental data very well. Finally, Figure 14 presents a comparison between theoretical predictions and excess volume data for carbon dioxide (1) + ethane (2) binary mixtures measured by Wormald and Hodgetts at 291.6 K and over a range of pressures.[120] The SAFT-VRX equation is found to predict the excess volumes in excellent agreement with the experimental data over a wide range of pressures and densities.

4. Conclusions

We have derived the crossover SAFT-VR (SAFT-VRX) equation of state for mixtures by combining the SAFT-VR equation with the crossover approach of Kiselev.[43] The van der

Waals one-fluid mixing rule is implemented, and correlations between the parameters for mixtures and pure fluids are formulated to minimize the need to fit to the experimental data. We have applied the SAFT-VRX equation to predict the thermodynamic properties of 14 binary *n*-alkane and 4 carbon dioxide + *n*-alkane binary mixtures in the one- and two-phase regions. We have demonstrated that the SAFT-VRX approach provides very good predictions of the whole phase diagram, including the gas−liquid critical lines and single-phase $p\upsilon T$ behavior, for the binary mixtures studied. We also have shown that the SAFT-VRX approach, using transferable parameters fitted to a single binary mixture, is able to describe the experimental coexisting densities, compressibility, $p\rho T$ surfaces, and excess volumes over a wide range of state conditions for the carbon dioxide + *n*-alkane binary mixtures studied. In the present work, we limit the application of the SAFT-VRX equation to binary mixtures and focus on the gas−liquid critical locus of those mixtures. In general, the SAFT-VRX approach can also be applied to study multicomponent mixtures and the transitions between other types of phase behavior.

Acknowledgment. L.S., H.Z., and C.M.C. acknowledge support from the U. S. National Science Foundation under grant nos. CTS-0319062 and CTS-0452688. S.B.K. acknowledges the U. S. Department of Energy, Office of Basic Energy Sciences, under grant no. DE-FG03-95ER14568.

References and Notes

(1) Prausnitz, J. M.; Lichtenthaler, R. N.; Gomes de Azevedo, E. *Molecular Thermodynamics of Fluid-Phase Equilibria*, 2nd ed.; Prentice Hall: New Jersey, 1999.
(2) McCabe, C.; Kiselev, S. B. *Fluid Phase Equilib.* **2004**, *219*, 3.
(3) McCabe, C.; Kiselev, S. *Ind. Eng. Chem. Res.* **2004**, *43*, 2839.
(4) Redlich, O.; Kwong, J. N. S. *Chem. Rev.* **1949**, *44*, 233.
(5) Soave, G. S. *Chem. Eng. Sci.* **1972**, *27*, 1197.
(6) Peng, D.-Y.; Robinson, D. B. *Ind. Eng. Chem. Fundam.* **1976**, *15*, 59.
(7) Anderko, A. In *Equations of State for Fluids and Fluid Mixtures*; Sengers, J. V., Kayser, R. F., Peters, C. J., White, H. J. J., Eds.; Elsevier: Amsterdam, 2000; Vol. I, p 75.
(8) Chapman, W. G.; Gubbins, K. E.; Jackson, G.; Radosz, M. *Fluid Phase Equilib.* **1989**, *52*, 31.
(9) Chapman, W. G.; Gubbins, K. E.; Jackson, G.; Radosz, M. *Ind. Eng. Chem. Res.* **1990**, *29*, 1709.
(10) Wertheim, M. S. *J. Stat. Phys.* **1984**, *35*, 19.
(11) Wertheim, M. S. *J. Stat. Phys.* **1984**, *35*, 35.
(12) Wertheim, M. S. *J. Stat. Phys.* **1986**, *42*, 459.
(13) Wertheim, M. S. *J. Stat. Phys.* **1986**, *42*, 477.
(14) Wertheim, M. S. *J. Chem. Phys.* **1986**, *85*, 2929.
(15) Wertheim, M. S. *J. Chem. Phys.* **1987**, *87*, 7323.
(16) Muller, E. A.; Gubbins, K. E. *Ind. Eng. Chem. Res.* **2001**, *40*, 2193.
(17) Gil-Villegas, A.; Galindo, A.; Whitehead, P. J.; Mills, S. J.; Jackson, G. *J. Chem. Phys.* **1997**, *106*, 4168.
(18) Galindo, A.; Davies, L. A.; Gil-Villegas, A.; Jackson, G. *Mol. Phys.* **1998**, *93*, 241.
(19) Gil-Villegas, A.; Galindo, A.; Whitehead, P. J.; Mills, S. J.; Jackson, G.; Burgess, A. N. *J. Chem. Phys.* **1997**, *106*, 4168.
(20) McCabe, C.; Galindo, A.; Gil-Villegas, A.; Jackson, G. *Int. J. Thermophys.* **1998**, *19*, 1511.
(21) McCabe, C.; Gil-Villegas, A.; Jackson, G. *J. Phys. Chem. B* **1998**, *102*, 4183.
(22) McCabe, C.; Jackson, G. *Phys. Chem. Chem. Phys.* **1999**, *1*, 2057.
(23) Filipe, E. J. M.; de Azevedo, E.; Martins, L. F. G.; Soares, V. A. M.; Calado, J. C. G.; McCabe, C.; Jackson, G. *J. Phys. Chem. B* **2000**, *104*, 1315.
(24) Filipe, E. J. M.; Martins, L. F. G.; Calado, J. C. G.; McCabe, C.; Jackson, G. *J. Phys. Chem. B* **2000**, *104*, 1322.
(25) McCabe, C.; Galindo, A.; Cummings, P. T. *J. Phys. Chem. B* **2003**, *107*, 12307.
(26) McCabe, C.; Galindo, A.; Garcia-Lisbona, M. N.; Jackson, G. *Ind. Eng. Chem. Res.* **2001**, *40*, 3835.
(27) Paricaud, P.; Galindo, A.; Jackson, G. *Fluid Phase Equilib.* **2002**, *194*−*197*, 87.
(28) McCabe, C.; Galindo, A.; Gil-Villegas, A.; Jackson, G. *J. Phys. Chem. B* **1998**, *102*, 8060.
(29) McCabe, C.; Dias, L. M. B.; Jackson, G.; Filipe, E. J. M. *Phys. Chem. Chem. Phys.* **2001**, *3*, 2852.
(30) Bonifacio, R. P.; Filipe, E. J. M.; McCabe, C.; Gomes, M. F. C.; Padua, A. A. H. *Mol. Phys.* **2002**, *100*, 2547.
(31) Morgado, P.; McCabe, C.; Filipe, E. J. M. *Fluid Phase Equilib.*, in press.
(32) Blas, F. J.; Galindo, A. *Fluid Phase Equilib.* **2002**, *194*−*197*, 501.
(33) Galindo, A.; Blas, F. J. *J. Phys. Chem. B* **2002**, *106*, 4503.
(34) Galindo, A.; Gil-Villegas, A.; Whitehead, P. J.; Jackson, G.; Burgess, A. N. *J. Phys. Chem. B* **1998**, *102*, 7632.
(35) Galindo, A.; Gil-Villegas, A.; Jackson, G.; Burgess, A. N. *J. Phys. Chem. B* **1999**, *103*, 10272.
(36) Gil-Villegas, A.; Galindo, A.; Jackson, G. *Mol. Phys.* **2001**, *99*, 531.
(37) Scott, R. L.; van Konynenburg, P. H. *Discuss. Faraday Soc.* **1970**, *49*, 87.
(38) van Konynenburg, P. H.; Scott, R. L. *Philos. Trans. R. Soc. London, Ser. A* **1980**, *298*, 495.
(39) McCabe, C.; Gil-Villegas, A.; Jackson, G. *J. Phys. Chem. B* **1998**, *102*, 4183.
(40) McCabe, C.; Galindo, A.; Gil-Villegas, A.; Jackson, G. *Int. J. Thermophys.* **1998**, *19*, 1511.
(41) McCabe, C.; Galindo, A.; Gil-Villegas, A.; Jackson, G. *J. Phys. Chem. B* **1998**, *102*, 8060.
(42) Sengers, J. V.; Levelt Sengers, J. M. H. *Annu. Rev. Phys. Chem.* **1986**, *37*, 189.
(43) Kiselev, S. B. *Fluid Phase Equilib.* **1998**, *147*, 7.
(44) Kiselev, S. B.; Ely, J. F. *J. Chem. Phys.* **2003**, *119*, 8645.
(45) Chapela, G. A.; Rowlinson, J. S. *J. Chem. Soc., Faraday Trans. 1* **1974**, *70*, 584.
(46) Levelt Sengers, J. M. H.; Hocken, R.; Sengers, J. V. *Phys. Today* **1977**, *30*, 42.
(47) Albright, P. C.; Sengers, J. V.; Nicoll, J. F.; Leykoo, M. *Int. J. Thermophys.* **1986**, *7*, 75.
(48) Van Pelt, A.; Jin, G. X.; Sengers, J. V. *Int. J. Thermophys.* **1994**, *15*, 687.
(49) Wyczalkowska, A. K.; Anisimov, M. A.; Sengers, J. V. *Fluid Phase Equilib.* **1999**, *160*, 523.
(50) Kiselev, S. B.; Ely, J. F. *Ind. Eng. Chem. Res.* **1999**, *38*, 4993.
(51) Kiselev, S. B.; Friend, D. G. *Fluid Phase Equilib.* **1999**, *162*, 51.
(52) Vanpelt, A.; Jin, G. X.; Sengers, J. V. *Int. J. Thermophys.* **1994**, *15*, 687.
(53) Kiselev, S. B.; Ely, J. F.; Abdulagatov, I. M.; Magee, J. W. *Int. J. Thermophys.* **2000**, *21*, 1373.
(54) Kiselev, S. B.; Ely, J. F. *Fluid Phase Equilib.* **2000**, *174*, 93.
(55) Kiselev, S. B.; Ely, J. F.; Adidharma, H.; Radosz, M. *Fluid Phase Equilib.* **2001**, *183*−*184*, 53.
(56) Huang, S. H.; Radosz, M. *Ind. Eng. Chem. Res.* **1990**, *29*, 2284.
(57) Huang, S. H.; Radosz, M. *Ind. Eng. Chem. Res.* **1991**, *30*, 1994.
(58) Kiselev, S. B.; Ely, J. F. *Fluid Phase Equilib.* **2000**, *174*, 93.
(59) Hu, Z.-Q.; Yang, J.-C.; Li, Y.-G. *Fluid Phase Equilib.* **2003**, *205*, 1.
(60) McCabe, C.; Kiselev, S. B. *Ind. Eng. Chem. Res.* **2004**, *43*, 2839.
(61) McCabe, C.; Kiselev, S. B. *Fluid Phase Equilib.* **2004**, *219*, 3.
(62) Parola, A.; Reatto, L. *Phys. Rev. Lett.* **1984**, *53*, 2417.
(63) Parola, A.; Reatto, L. *Phys. Rev. A* **1985**, *31*, 3309.
(64) Parola, A.; Meroni, A.; Reatto, L. *Int. J. Thermophys.* **1989**, *10*, 345.
(65) Tau, M.; Parola, A.; Pini, D.; Reatto, L. *Phys. Rev. E* **1995**, *52*, 2644.
(66) Reatto, L.; Parola, A. *J. Phys.: Condens. Matter* **1996**, *8*, 9221.
(67) White, J. A.; Zhang, S. *J. Chem. Phys.* **1990**, *103*, 1922.
(68) White, J. A.; Zhang, S. *J. Chem. Phys.* **1993**, *99*, 2012.
(69) White, J. A. *J. Chem. Phys.* **1999**, *111*, 9352.
(70) White, J. A. *J. Chem. Phys.* **2000**, *112*, 3236.
(71) White, J. A. *Int. J. Thermophys.* **2001**, *22*, 1147.
(72) Jiang, J.; Prausnitz, J. M. *J. Chem. Phys.* **1999**, *111*, 5964.
(73) Jiang, J.; Prausnitz, J. M. *Fluid Phase Equilib.* **2000**, *169*, 127.
(74) Jiang, J.; Prausnitz, J. M. *AIChE J.* **2000**, *46*, 2525.
(75) Cai, J.; Prausnitz, J. M. *Fluid Phase Equilib.* **2004**, *219*, 205.
(76) Llovell, F.; Pàmies, J. C.; Vega, L. F. *J. Chem. Phys.* **2004**, *121*, 10715.
(77) Leung, S. S.; Griffiths, R. B. *Phys. Rev. A* **1973**, *8*, 2670.
(78) Rainwater, J. C.; Moldover, M. R. In *Chemical Engineering at Supercritical Fluid Conditions*; Paulaitis, M. E., Penninger, J. M. L., Gray, R. D., Davidson, P., Eds.; Ann Arbor Science: Ann Arbor, MI, 1983.
(79) Moldover, M. R.; Rainwater, J. C. *J. Chem. Phys.* **1988**, *88*, 7772.
(80) Rainwater, J. C. Vapor-Liquid Equilibrium and the Modified Leung−Griffiths Model. In *Supercritical Fluid Technology*; CRC Press: Boca Raton, FL, 1991; p 57.
(81) Jin, G. X.; Tang, S.; Sengers, J. V. *Phys. Rev. E* **1993**, *47*, 388.
(82) Povodyrev, A. A.; Jin, G. X.; Kiselev, S. B.; Sengers, J. V. *Int. J. Thermophys.* **1996**, *17*, 909.

(83) Belyakov, M. Y.; Kiselev, S. B.; Rainwater, J. C. *J. Chem. Phys.* **1997**, *107*, 3085.
(84) Kiselev, S. B. *Fluid Phase Equilib.* **1997**, *128*, 1.
(85) Kiselev, S. B.; Kulikov, V. D. *Int. J. Thermophys.* **1997**, *18*, 1143.
(86) Kiselev, S. B.; Huber, M. L. *Int. J. Refrig.* **1998**, *21*, 64.
(87) Kiselev, S. B.; Rainwater, J. C. *J. Chem. Phys.* **1998**, *109*, 643.
(88) Kiselev, S. B.; Rainwater, J. C.; Huber, M. L. *Fluid Phase Equilib.* **1998**, *151*, 469.
(89) Belyakov, M. Y.; Kiselev, S. B.; Rainwater, J. C. *J. Chem. Phys.* **1997**, *107*, 3085.
(90) Kiselev, S. B. *Fluid Phase Equilib.* **1997**, *128*, 1.
(91) Kiselev, S. B.; Rainwater, J. C. *Fluid Phase Equilib.* **1997**, *141*, 129.
(92) Kiselev, S. B.; Kulikov, V. D. *Int. J. Thermophys.* **1997**, *18*, 1143.
(93) Kiselev, S. B.; Rainwater, J. C.; Huber, M. L. *Fluid Phase Equilib.* **1998**, *150*−*151*, 469.
(94) Kiselev, S. B.; Rainwater, J. C. *J. Chem. Phys.* **1998**, *109*, 643.
(95) Kiselev, S. B.; Huber, M. L. *Int. J. Refrig.* **1998**, *21*, 64.
(96) Kiselev, S. B.; Ely, J. F. *J. Chem. Phys.* **2003**, *119*, 8645.
(97) Hansen, J. P.; McDonald, I. P. *Theory of Simple Liquids*, 2nd ed.; Academic Press: London, 1986.
(98) Barker, J. A.; Henderson, D. *J. Chem. Phys.* **1967**, *47*, 2856.
(99) Barker, J. A.; Henderson, D. *Rev. Mod. Phys.* **1975**, *48*, 587.
(100) Leonard, P. J.; Henderson, D.; Barker, J. A. *Trans. Faraday Soc.* **1970**, *66*, 2439.
(101) Boublik, T. *J. Chem. Phys.* **1970**, *53*, 471.
(102) Mansoori, G. A.; Carnahan, N. F.; Starling, K. E.; Leland, T. W. *J. Chem. Phys.* **1971**, *54*, 1523.
(103) Lee, L. L. *Molecular Thermodynamic of Nonideal Fluids*; Butterworth: London, 1988.
(104) Rowlinson, J. S.; Swinton, F. L. *Liquid and Liquid Mixtures*, 3rd ed.; Butterworth Scientific: London, 1982.
(105) Reed, T. M.; Gubbins, K. E. *Applied Statistical Mechanics*; McGraw-Hill: New York, 1973.
(106) Patel, B.; Docherty, H.; Varga, S.; Galindo, A.; Maitland, G. C. *Mol. Phys.* **2005**, *103*, 129.
(107) Levelt Sengers, J. M. H.; Chang, R. F.; Morrison, G. In *Equation of State: Theories and Applications*; Chao, K. C., Robinson, R. L., Jr., Eds.; ACS Symposium Series 330; American Chemical Society, Washington, DC, 1986; p 110.
(108) Anisimov, M. A.; Kiselev, S. B. In *Soviet Technology Reviews Section B Thermal Physics Reviews*; Scheindlin, A. E., Fortov, V. E., Eds.; Harwood Academic: New York, 1992; Vol. II.
(109) We note that the parameters listed in Table 1 for carbon dioxide differ from those reported in earlier work.[60] Since δ_r is very close to zero, in this work it has been set to zero, which reduces the total number of parameters by one.
(110) Sun, L.; Zhao, H.; Kiselev, S. B.; McCabe, C. *Fluid Phase Equilib.*, in press.
(111) Parrish, W. R. *Fluid Phase Equilib.* **1986**, *25*, 65.
(112) Hicks, C. P.; Young, C. L. *Chem. Rev.* **1975**, *75*, 119.
(113) Niesen, V. G. *J. Chem. Thermodyn.* **1989**, *21*, 915.
(114) Fredenslund, A.; Mollerup, J. *J. Chem. Soc., Faraday Trans. 1* **1974**, *70*, 1653.
(115) Horstmann, S.; Fischer, K.; Gmehling, J.; Kolar, P. *J. Chem. Thermodyn.* **2000**, *32*, 451.
(116) Weber, L. A. *Int. J. Thermophys.* **1992**, *13*, 1011.
(117) Lau, W.-W. R. A Continuously Weighed Pycnometer Providing Densities for CO_2 + Ethane Mixtures Between 240 and 350 K and Pressures up to 35 MPa. Texas A&M University, 1986.
(118) Tsuji, T.; Honda, S.; Kiaki, T.; Hongo, M. *J. Supercrit. Fluids* **1998**, *13*, 15.
(119) Kiran, E.; Pohler, H.; Xiong, Y. *J. Chem. Eng. Data* **1996**, *41*, 158.
(120) Wormald, C. J.; Hodgetts, R. W. *J. Chem. Thermodyn.* **1997**, *29*, 75.
(121) Vargaftik, N. B. *Handbook of Physical Properties of Liquids and Gases: Pure Substances and Mixtures*, 2nd ed.; Springer-Verlag: Berlin, 1983.
(122) Nysewander, C. N.; Sage, B. H.; Lacey, W. N. *Ind. Eng. Chem.* **1940**, *32*, 118.
(123) Grieves, R. B.; Thodas, C. *J. Appl. Chem.* **1963**, *13*, 466.
(124) Kay, W. B. *J. Chem. Eng. Data* **1970**, *15*, 46.
(125) Weise, H. C.; Jacobs, J.; Sage, B. H. *J. Chem. Eng. Data* **1970**, *15*, 82.
(126) Pak, S. C.; Kay, W. B. *Ind. Eng. Chem. Fundam.* **1972**, *11*, 255.
(127) Kay, W. B.; Genco, J.; Fichtner, D. A. *J. Chem. Eng. Data* **1974**, *19*, 275.